A Two-Stage Simultaneous Control Scheme for the Transient Angle Stability of VSG Considering Current Limitation and Voltage Support

Kun Sun, Wei Yao, *Senior Member, IEEE*, Jinyu Wen, *Member, IEEE*, and Lin Jiang, *Member, IEEE*

***Abstract*—Since the wide application of virtual synchronous generators (VSGs), the power grid faces great challenges in the safe and stable operation due to their limited thermal capacity and weak anti-disturbance ability. During transient period, for example, a fault occurs in the transmission line, the VSG may lose the transient angle stability and provoke the current hard limit. Even if the fault is cleared by tripping of line, it still faces the problem of instability and voltage dips. To address this problem, in this paper, the post-fault large-signal model of VSG is derived first via the travelling waves based fault information acquisition. Subsequently, with the effect of both active and reactive power loops taken into account, a two-stage simultaneous control scheme is proposed for improving the transient stability of VSG, while considering the current limitation during fault state and voltage support after fault clearance. This method is fulfilled by mode switching and an additional feedback control based on the fault signal. Finally, the effectiveness of the proposed method under both symmetrical and asymmetrical faults is verified. Moreover, the application of the proposed method in a multiple VSGs system is also verified. Besides, the robustness to parameter mismatch and the feasible operating region for the method are discussed.**

***Index Terms*—virtual synchronous generator, large-signal model, fault, transient angle stability, current limitation, voltage support**

NOMENCLATURE

U_g, θ_g	grid voltage amplitude and phase angle
U_f, θ_f	fault point voltage amplitude and phase angle
U_{pcc}, θ_{pcc}	fault point voltage amplitude and phase angle
δ	phase difference between grid and VSG
L_f, C_f	filter inductance and capacitor of VSG
Z_1, Z_2	parallel-circuit transmission lines impedance
Z_{21}, Z_{22}	line impedance on either side of the fault point
Z_T, Z_f	transformer impedance and fault impedance
m, n	line length on either side of the fault point
u_f, u_q	refracted and reflected wave from fault point
J, D_p	virtual inertia and damping coefficient of VSG
R, R', R''	system total resistance during normal state, fault state and O/S state
X, X', X''	system total inductance during normal state, fault state and O/S state
E, E', E''	terminal voltage of VSG during normal state, fault state and O/S state
θ_{vsg}, θ_{vsg}', θ_{vsg}''	phase angle of VSG during normal state, fault state and O/S state
I, I', I''	output current of VSG during normal state, fault state and O/S state
P_e, P_e', P_e''	output active power of VSG during normal state, fault state and O/S state
P_0, P_0', P_0''	active power reference of VSG during normal state, fault state and O/S state
K_q, K_q', K_q''	reactive droop coefficient of VSG during normal state, fault state and O/S state
Q_e, Q_0	output reactive power and reference of VSG
θ_{set}, E_{set}, I_{set}	set value of θ_{vsg}, E, I of VSG during transient

Superscript

+, -	positive and negative components

Subscripts

d, q	d, q axis components in dq frame

I. Introduction

With the increasing application of renewable energy resources, the power grids are interfaced by voltage source converters (VSCs) with the flexibility and full controllability [1]. To solve the reduced inertia and less damping caused by the connection of VSCs, virtual synchronous generators (VSGs) are designed to mimic the output characteristics of traditional synchronous generators (SGs) [2]. While benefiting from the SG-like operation, VSGs also suffer from the transient angle stability problem after a large-signal disturbance, like severe grid voltage dips, fault on transmission lines or tripping of line. Moreover, VSGs are a type of grid-forming VSCs with low over-current capabilities and thus are susceptible to physical

Manuscript received March 06, 2021; revised July 22, 2021 and September 05, 2021; accepted October 17, 2021. This work was supported by the National Natural Science Foundation of China under Grant 52022035. Paper no. TPWRS-00357-2021. (*Corresponding author: Wei Yao*.)

K. Sun, W. Yao, and J. Wen are with State Key Laboratory of Advanced Electromagnetic Engineering and Technology, School of Electrical and Electronic Engineering, Huazhong University of Science and Technology, Wuhan, 430074, China. (email: kunsun93@foxmail.com; w.yao@hust.edu.cn; jinyu.wen@hust.edu.cn)

L. Jiang is with the Department of Electrical Engineering and Electronics, University of Liverpool, Liverpool, U.K. (e-mail: ljiang@liv.ac.uk).

damages under severe disturbances [3]. But the current limitation units may lead to instability problems of VSGs in turn [4]. Therefore, both the transient stability and current limitation during fault state of VSGs attracts increasing research interests recently. In addition, the transient stability and voltage recovery of VSGs after fault clearance are also concerned.

Substantial research efforts have been devoted to VSGs, with the main focus on small-signal analysis [5]. However, it is not applicable if the equilibrium operating point is changed by a large-signal disturbance. Thus, the transient angle stability of VSGs, which describes the ability to maintain synchronization with the grid, is worth of studying. To enhance the transient stability of VSGs, two categories of methods can be adopted. One is the change of power references, and the other is the modification of the control loops or parameters [6]. A method of reducing active power reference is adopted in [7] to solve the active power imbalance due to the analysis with power-angle curve. In [8], the effect of Q-V droop loop is studied, which would deteriorate the stability of VSGs caused by the positive feedback of the voltage control loop. It is concluded in [9] that the synchronization issues of grid-forming VSCs are determined by the transient response of both the active and reactive power loops. Besides, variable inertia coefficient and damping adaptation methods are proposed to improve stability margin of the system [10]. In addition, transient stability of multiple VSGs is also addressed in [11], [12].

In addition, the current limitation of VSGs is important. Unlike the SGs, the converter has a rigid current limit to avoid overcurrent damage. To guarantee secure operation of VSGs during fault state, varieties of current limiting strategies have been proposed. One basic strategy is to limit the current directly with a saturation block, and then the converter works as a constant current source during fault state [4]. However, the converter would lose synchronization due to the uncontrollable outer loops and wind-up in them [13]. To maintain the synchronization during fault state, the methods of mode switching from voltage control to grid-following control are adopted in [14], [15]. However, a backup PLL is necessary, and there is a problem to switch back after fault clearance. Even worse, the robust properties of the grid-forming control are lost during fault state. To avoid this switching, the virtual impedance is implemented to limit the current by reducing the voltage reference [16], [17]. Nevertheless, the dynamic performance of VSGs may be influenced by the virtual impedance, which may limit its usefulness. Besides, the current limitation can also be fulfilled by the modification of power references [18] or droop controller parameters [19].

For the sake of stable and safe operation of VSGs, lots of researches have been done. But there are still some problems not extensively studied in the references. Firstly, the transient stability and the current limitation during fault state should be considered simultaneously. However, the methods in [7]-[12] for the transient stability may provoke the current limitation. In contrast, the use of the current limiter drives the converter into transient instability area easily during fault state [15]. And the activation of the virtual impedance results in a decrease of the critical clearing time [19]. Secondly, the operating state with one of the parallel-circuit lines out of service (O/S state) after fault clearance is rarely taken into account in the above references. This state may also cause the transient instability and internal voltage dips of VSGs due to the increase of system impedance, which should be investigated as well. Note that the transient stability in O/S state is considered with a mode-switching control in [20], which could ride through even without an equilibrium point according to a switched control gain k in the forward path of the active power loop. However, the voltage recovery in O/S state is not considered in this method. Thirdly, the power angle and output current during fault state cannot be accurately controlled at the same time in the above methods. For instance, the typical challenge of the method in [7], [8] lies in how to quantify the changes of power references. In [20], the power angle is oscillated, since the mode is keep switching without an equilibrium point.

In short, how to accurately and simultaneously control the transient stability of VSG while considering the current limiting during fault state and the voltage support after fault clearance should be explored. To solve the above problems, this paper proposes a two-stage simultaneous control scheme of VSG for a fault in the transmission line. Based on the fault information obtained by TWs method, the post-fault large-signal model of VSG can be built. By taking the effect of both active and reactive power control loops into account, the transient angle stability and current limitation of the VSG during fault state can be controlled precisely at the same time. In addition, the transient stability and internal voltage recovery of the VSG are also guaranteed during O/S state. The main contributions of this paper are listed as follows:

- A two-stage control scheme for the transient angle stability of VSG is proposed, while considering the current limitation during fault state and voltage support during O/S state. The method is fulfilled by mode switching and an additional feedback control with the TWs-based fault information acquisition.
- With the effect of both active and reactive power loops taken into account, the transient angle stability and the current limitation of VSG during fault state can be guaranteed simultaneously and precisely by the proposed method. Similarly, the phase angle and the internal voltage of VSG after fault clearance can be controlled at the meanwhile.
- The robustness to parameters mismatch originated from fault location and calculation is analyzed. And the feasible operating region of the proposed method during fault state is investigated as well.
- In particular, the effectiveness of the proposed method under asymmetric fault is verified as well. In addition, the application of the proposed method for a multiple VSGs system is analyzed.

The rest of the paper is organized as follows. In Section II, the large-signal model of VSG is derived. In Section III, a two-stage simultaneous control scheme is proposed for the transient stability of VSG while considering the current limitation and voltage support. The effect of the proposed method is analyzed by case studies in Section IV, where the robustness and feasible operating region for the proposed method are discussed as well. In addition, the validation of the proposed method under asymmetric fault and for multiple VSGs are carried out. Conclusions are drawn in Section V.

II. Large-Signal Modeling of VSG During Fault State and O/S State

In this Section, the system configuration and control structure of VSG are illustrated. Based on that, the large-signal models of VSG during fault state and O/S state are derived, respectively.

A. System Configuration

The single-line diagram of a grid-connected VSG and its control structure are shown in Fig. 1. The VSG is connected to the grid through a transformer and parallel-circuit transmission lines. Z_1, Z_2 represent for the line impedance. Z_T is the transformer's leakage impedance. L_f, C_f are the inductance and capacitor of the LC filter for VSG. When a grounding fault occurs in one of the lines, Z_f denotes the grounding impedance, while Z_{21}, Z_{22} represent the line impedance on either side of the fault point. The grid voltage is represented by a vector $\boldsymbol{U}_g$ with amplitude U_g and phase θ_g. Similarly, the voltage at the fault point is represented as $\boldsymbol{U}_f$ with amplitude U_f and phase θ_f.

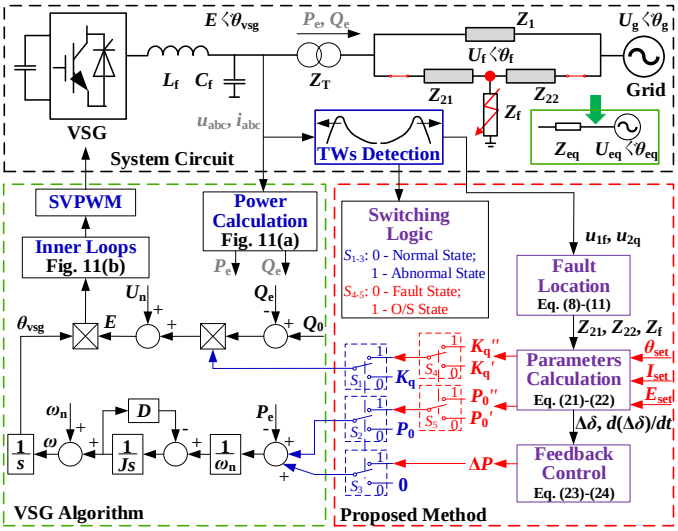

Fig. 1. System structure and the proposed method of VSG.

The control structure of VSG can be divided into two parts. The active power control loop aims to mimic mechanical rotor motion of SGs. The reactive power control loop is used to regulate output reactive power. The phase and the voltage amplitude commands, θ_{vsg} and E, are produced by the control loops respectively, and then combined to generate the voltage reference vector $\boldsymbol{E}$. In general, the dynamic of the outer power loop is over ten times slower than that of the inner voltage and current loop [21], [22]. Due to the decoupled timescales, the outer and inner loop can be evaluated individually. Thus, the inner voltage and current dual-loops can be regarded as a unity gain with an ideal reference tracking, while the transient stability issue is mainly determined by the outer power control loop. This simplification used in this paper has been validated in [7-9], [18-20]. Similarly, the dynamic characteristics of the inductor and the capacitor can also be ignored.

B. Mathematical Model of VSG in Normal State

As shown in Fig. 1, $\boldsymbol{E}$ is VSG's internal voltage which is expressed as $E\angle\theta_{vsg}$. $\boldsymbol{U}_g$ is the grid voltage which is expressed as $U_g\angle\theta_g$. Taking $\boldsymbol{U}_g$ as a reference, the power angle δ is defined as the phase difference between $\boldsymbol{U}_g$ and $\boldsymbol{E}$, which is $\delta = \theta_{vsg} - \theta_g$. ω_n is the rated angular frequency. The swing equation of the active power control loop can be modelled as

$$J\ddot{\delta} = -D\dot{\delta} + (P_0 - P_e) \tag{1}$$

where, J is the virtual inertia, D is the damping coefficient, P_0 and P_e are the active power reference and the output active power of the VSG. Besides, the Q-V droop of reactive power control loop is modelled as

$$E = K_q(Q_0 - Q_e) + U_n \tag{2}$$

where, U_n is the nominal voltage magnitude, K_q is the Q-V droop coefficient. Q_0 and Q_e are the reactive power reference and the output reactive power of the VSG.

Normally, the total system impedance can be expressed as $Z=Z_1||Z_2+Z_T=R+j(X+X_T)$. And then the output active power and reactive power of the VSG can be expressed as

$$P_e = -\alpha U_g E\cos\delta + \beta U_g E\sin\delta + \alpha E^2 \tag{3}$$

$$Q_e = -\alpha U_g E\sin\delta - \beta U_g E\cos\delta + \beta E^2 \tag{4}$$

where $\alpha = R/[R^2+(X+X_T)^2]$, $\beta = X/[R^2+(X+X_T)^2]$.

By combining (3) and (4), the steady-state output current of VSG can be derived as

$$I = \left|\frac{E-U_g}{Z}\right| = \frac{1}{\sqrt{R^2+(X+X_T)^2}}\cdot\sqrt{U_g^2+E^2-2U_gE\cos\delta} \tag{5}$$

By substituting (4) into (2), the relationship between E and δ can be revealed as (6)

$$E = \frac{K_qU_g(\alpha\sin\delta+\beta\cos\delta)-1+\sqrt{[K_qU_g(\alpha\sin\delta+\beta\cos\delta)-1]^2+4\beta K_q(U_n+K_qQ_0)}}{2\beta K_q} \tag{6}$$

By substituting (6) into (3), the relationship between P_e and δ can be revealed. Thus, the P_e - δ curve with different U_g, K_q can be plotted. By combining (1) and (3), the second order nonlinear differential equation of the VSG can be derived as

$$J\ddot{\delta} = -D\dot{\delta} + [P_0 - (-\alpha U_gE\cos\delta + \beta U_gE\sin\delta + \alpha E^2)] \tag{7}$$

Based on (7) with the E represented by (6), the dynamic characteristics of this second-order nonlinear dynamic system can be described. However, the analytic solution of (7) is hard to obtain. Instead, the phase portrait, which is a graphical solution of (7), can provide a simpler and more intuitive result.

C. Mathematical Model of VSG During Fault State

The mathematical model of VSG in normal state is derived in (3)-(7). However, it is no longer applicable during fault state since the system topology is changed after fault occurs. To obtain the real-time fault information like Z_{21}, Z_{22}, Z_f for the large-signal model of VSG during fault state, a suitable method for on-line fault location and fault impedance measurement is necessary.

Travelling waves (TWs) based method is adopted due to its advantages such as high accuracy, speed and reliability [23]-[25]. In particular, since the velocity of propagation near the speed of light, the fault information acquisition can be achieved by TWs method within 0.5 μs for 1 MHz sampling frequency. Nowadays TWs method has been widely applied in practice, especially used in high voltage transmission line fault location. Therefore, the accuracy and speed requirement is

guaranteed by TWs method for the further control in this paper. Note that only the system topology nearby the fault line is changed and needs to be updated, while the other regions of the system remain unchanged. Thus, the fault information acquisition can be realized timely, and then the further parameters calculation can be implemented instantaneously.

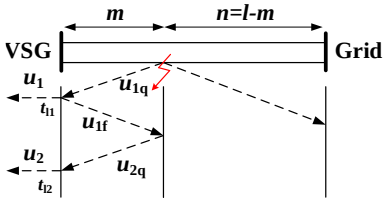

Fig. 2. Time-space diagram for a fault in the transmission line.

As shown in Fig. 2, l is the line length while m and n are the fault distance seeing from the ends. When a fault occurs on one of the lines, the fault point will generate TWs transmitted to both ends. The initial forward TW u_{1q} is reflected at the VSG side which generate the refracted wave u_1 and reflected wave u_{1f}. After a delay of $2m/v$, u_{1f} is reflected as u_{2q} at the fault point and then arrives at the VSG side again where it is refracted as u_2. The propagation process on the grid side is similar. Due to the above analysis, a single-end method is adopted to calculate the fault distance, by detecting the time different between u_1 and u_2. The fault distance and the line impedances on either side of the fault point can be derived as

$$m=\frac{1}{2}(t_{l2}-t_{l1})v,\quad n=l-m \tag{8}$$

$$Z_{21}=m(r_1+\mathrm{j}\omega l_1),\quad Z_{22}=n(r_1+\mathrm{j}\omega l_1) \tag{9}$$

where t_{l1} and t_{l2} are the arrival times of u_1 and u_2 at the VSG terminal. $v=\omega/[0.5\omega c_1(\omega l_1+\sqrt{r_1^2+\omega^2 l_1^2})]^{1/2}$ is propagation speed while r_1, l_1, c_1 are the positive distributed parameters of line resistance, inductance, capacitance per unit length. Note that the line in this study is shorter than 100 km, so the lumped parameters are applicable for the further parameters design since the main concern is the transient characteristics of VSG.

In addition, the fault impedance Z_f can be derived based on the relationship between u_{1f} and u_{2q} by reflection laws [24].

$$Z_{\mathrm{f}}=-\frac{1}{2}Z_{\mathrm{c}}\left(\frac{u_{1\mathrm{f}}\,\mathrm{e}^{-2\gamma m}}{u_{2\mathrm{q}}}+1\right) \tag{10}$$

where $Z_{\mathrm{c}}=\sqrt{(r_1+\mathrm{j}\omega l_1)/\mathrm{j}\omega c_1}$, $\gamma=\sqrt{(r_1+\mathrm{j}\omega l_1)\,\mathrm{j}\omega c_1}$ are the line wave impedance and the TWs attenuation coefficient. Note that to detect and extract the TWs accurately, the signals should be further processed by the modal and wavelet transform for decoupling and noise elimination.

With the fault information Z_{21}, Z_{22}, Z_f acquired from the TWs method, the large-signal model of VSG during fault state can be built by the equivalent circuit method. A delta-star transformation is adopted first, and then yields the Thévenin equivalent circuit seeing from the VSG side towards the grid side [26]. Thus, the system circuit during fault state is transformed to the equivalent circuit shown in the green block in Fig. 1, which is as where the equivalent circuit parameters can be derived as

$$\begin{cases}\boldsymbol{U}_{\mathbf{eq}}=\dfrac{Z_{21}}{Z_1+Z_{21}}\boldsymbol{U}_{\mathbf{g}}+\dfrac{Z_1}{Z_1+Z_{21}}\boldsymbol{U}_{\mathbf{f}}\\ Z_{\mathrm{eq}}=\dfrac{Z_1Z_{21}}{Z_1+Z_{21}}\end{cases} \tag{11}$$

where $\boldsymbol{U}_{\mathbf{eq}}$ and Z_{eq} are the equivalent grid voltage vector and impedance in the Thévenin equivalent circuit. In particular, as to a symmetrical three-phase-to-ground fault, the derivation of the equivalent circuit parameters in (11) can be further simplified with the detection of fault impedance Z_f.

$$\begin{cases}\boldsymbol{U}_{\mathbf{eq}}=\dfrac{Z_{21}Z_{22}+2Z_2Z_{\mathrm{f}}}{Z_1Z_{22}+Z_{21}Z_{22}+2Z_2Z_{\mathrm{f}}}\boldsymbol{U}_{\mathbf{g}}\\ Z_{\mathrm{eq}}=\dfrac{Z_1Z_{21}+2Z_2Z_{\mathrm{T}}+(Z_{21}Z_{22}+2Z_2Z_{\mathrm{f}})\,\|\,Z_1Z_{22}}{2Z_2}\end{cases} \tag{12}$$

Thus, the steady-state output current of VSG during fault state is expressed as

$$I'=\left|\frac{E'-U_{\mathrm{eq}}}{Z'}\right|=\frac{1}{\sqrt{R'^2+X'^2}}\cdot\sqrt{U_{\mathrm{eq}}{}^2+E'^2-2U_{\mathrm{eq}}E'\cos\delta'} \tag{13}$$

where $Z'=Z_{\mathrm{eq}}+Z_{\mathrm{T}}=R'+\mathrm{j}X'$ is the total system impedance. The equivalent power angle δ' during fault state is changed to the phase difference between $\boldsymbol{U}_{\mathbf{eq}}$ and $\boldsymbol{E}'$, that is $\delta'=\theta_{\mathrm{vsg}}'-\theta_{\mathrm{eq}}$. And then the relationship between I', δ' and E' during fault state can be directly analyzed by (13), which is derived as

$$E'=U_{\mathrm{eq}}\cos\delta'+\sqrt{I'^2(R'^2+X'^2)-U_{\mathrm{eq}}{}^2\sin\delta'^2} \tag{14}$$

And the relationship between K_q' and E' during fault state can be derived according to (6).

$$K_{\mathrm{q}}'=\frac{U_{\mathrm{n}}-E'}{\beta'E'^2-E'U_{\mathrm{eq}}(\alpha'\sin\delta'+\beta'\cos\delta')-Q_0} \tag{15}$$

where $\alpha'=R'/(R'^2+X'^2)$, $\beta'=X'/(R'^2+X'^2)$.

Meanwhile, the output active power of the VSG during fault state can be rewritten as

$$P_{\mathrm{e}}'=-\alpha'U_{\mathrm{eq}}E'\cos\delta'+\beta'U_{\mathrm{eq}}E'\sin\delta'+\alpha'E'^2 \tag{16}$$

Thereby, during fault state, the VSG's second order nonlinear differential equation in (7) are modified with P_e, δ replaced by P_e', δ'. With this equivalent method, the transient stability of VSG during fault state can be further analyzed and the related improvement strategy can be explored.

D. Mathematical Model of VSG During O/S State

In addition, when the fault is cleared by tripping of the faulty line, the system is operated in O/S state with single-circuit line. Thereby, the mathematical model of VSG after fault clearance is derived as follows. Compared with the normal state, the total system impedance is changed to $Z''=Z_1+Z_{\mathrm{T}}=R''+\mathrm{j}X''$. Thus, the steady-state output current of VSG in O/S state is expressed as

$$I''=\frac{1}{\sqrt{R''^2+X''^2}}\cdot\sqrt{U_{\mathrm{g}}{}^2+E''^2-2U_{\mathrm{g}}E''\cos\delta''} \tag{17}$$

where the power angle δ'' after fault clearance is the phase difference between $\boldsymbol{U}_{\mathbf{g}}$ and $\boldsymbol{E}''$, that is $\delta''=\theta_{\mathrm{vsg}}''-\theta_{\mathrm{g}}$. And then the corresponding E'', K_q'', P_e'' during O/S state are derived as

$$E''=U_{\mathrm{g}}\cos\delta''+\sqrt{I''^2(R''^2+X''^2)-U_{\mathrm{g}}{}^2\sin\delta''^2} \tag{18}$$

$$K_q'' = \frac{U_n - E''}{\beta'' E''^2 - E'' U_g(\alpha'' \sin\delta'' + \beta'' \cos\delta'') - Q_0} \quad (19)$$

$$P_e'' = -\alpha'' U_g E'' \cos\delta'' + \beta'' U_g E'' \sin\delta'' + \alpha'' E''^2 \quad (20)$$

where $\alpha'' = R''/(R''^2 + X''^2)$, $\beta'' = X''/(R''^2 + X''^2)$.

Note that the system structure and its mathematical model will return to the initial normal state after the line reclosing.

III. Proposed Two-Stage Simultaneous Control

In this Section, the control principle and algorithm of the proposed method are introduced. In particular, the parameters design and the feedback control during fault state and O/S state are well illustrated.

A. Control Principle of the Proposed Method

Before introducing the proposed method, the main problems of VSGs under a large disturbance are reminded again, which are the transient instability and overcurrent.

The transient angle stability mechanism is explained as follows. Generally, the transient angle stability of VSG is dependent on the dynamic response of δ under a large disturbance. The VSG will be stable if δ can converge to a steady-state value, or will be unstable if δ diverges [7], [9], [20]. As shown in Fig. 3, the parallel transmission lines are initially both in service and the VSG operates at the equilibrium point *a*, where P_e=P_0 in the steady state. Taking the fault without equilibrium points as an example, VSG operates from initial equilibrium point *a* to the point *b* directly after fault occurs. The phase angle of VSG keeps increasing during fault state due to P_e'<P_0. Then the operating point of VSG is changed from *b* to *c*, which finally leads to the loss of synchronization of VSG without any control. In short, the operating trajectory is *a*→*b*→*c*. In addition, when the fault is cleared by tripping of line, normally there are two equilibrium points during O/S state. Note that the phase angle can only be decreased to the stable equilibrium point *d* with the fault clearance before the critical clearing angle δ_c considering the negative inertial effect of VSG. Otherwise, VSG may crossover the unstable equilibrium point *e*. Therefore, the fast fault clearance is of importance without any other control.

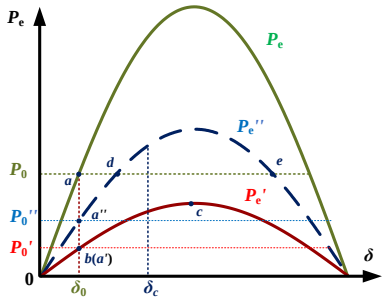

Fig. 3. P_e-δ curves during normal state, fault state and O/S state.

Even worse, a large fault current always accompanied under a grid fault, especially in a symmetrical three-phase-to-ground fault. The inverter may provoke the overcurrent limit and faces the physical damages. Therefore, the improvement of the transient stability and the current limitation must be both considered at the same time during fault state. In addition, when the fault is cleared by tripping of the faulty line, the output current of VSG will decrease from the limit value. However, it still faces the problem of transient instability due to the increase of system impedance after fault clearance. And the internal voltage of VSG is also lower than the rated voltage. Therefore, the transient stability and the internal voltage should be both considered in O/S state. Only when the line reclosing is successful will the system return to its initial normal state.

As far as we know, VSG control has two degrees of freedom. Thus, the simultaneous control of two objectives is theoretically feasible, which can be achieved by the original control loops of VSGs. The relationship between *E*, *I*, δ is expressed in (13)-(14), when two of them are given, another can be determined under the premise of knowing the fault information, which can be acquired from the TWs method. Therefore, during fault state, the control objectives are the phase angle θ_{vsg}' and output current amplitude I', which should be controlled as θ_{set} and I_{set} in the meantime. Similarly, the phase angle θ_{vsg}'' and internal voltage amplitude E'' should be controlled as θ_{set} and E_{set} after fault clearance.

Note that for the consideration of reaching both transient angle stability and current limitation faster, the phase angle of VSG should remain its original value during the transient. Normally, after the fault occurred, even if θ_{vsg} is convergent without any control, it still needs time to reach the new equilibrium point. As a comparison in Fig. 3, the initial power reference P_0 is changed to P_0' during fault state based on the basic idea, and thus the new equilibrium point *a'* is reached directly if the phase angle of VSG is controlled as its original value. And it is less likely to crossover the critical clearing angle δ_c. Similarly, the new equilibrium point *a''* is reached directly during O/S state, and it is less likely to approach the unstable equilibrium point. In short, the operating trajectory is *a*→*a'*(b)→*a''*. Therefore, VSG can reach a new equilibrium point during the transient process very fast with the basic idea, and thus the transient stability of VSG can be ensured. In addition, the current limitation can be realized fast simultaneously. The output current of VSG during the first cycle is fluctuated a lot with the increased θ_{vsg}. Since θ_{set} is set as its initial value and the trajectory of θ_{vsg} is barely budged, the output current of VSG can be stabilized to its limitation value fast as well.

B. Parameters Design of the Proposed Method

As shown in Fig. 1, during transient period, in order to control θ_{vsg}, *I* or *E* to the given value, two parameters in the active power and reactive power loops respectively should be regulated at the same time, which could be one of P_0, *D*, *J* and one of Q_0, K_q. According to (1)-(2), in the active power loop, P_0 is more convenient to be calculated than *D*, *J* due to their differential terms. And in the reactive power loop, K_q would influence the stability of VSGs caused by the positive feedback of the voltage control loop [9] while Q_0 may be regulated for other demands of the grid codes. Therefore, in the proposed method, P_0 and K_q are the chosen parameters need to be calculated and regulated. Similarly, the active power reference is changed with the variation of the droop coefficient in [27], which means the changing of power reference and droop coefficient can be realized simultaneously.

By combining (11)-(20) and the control principle proposed in Section III-A, the active power reference and Q-V droop coefficient of VSG are designed as subsection function in (21)-(22) in normal state, fault state and O/S state, respectively. To better illustrate the parameters design, the subsection function is expressed as Fig. 4(a). In normal state, P_0 and K_q are unchanged. Then P_0' and K_q' are applied in fault state to control θ_{vsg}' and I' to the set value θ_{set} and I_{set}. Similarly, P_0'' and K_q'' are applied in O/S state to control θ_{vsg}'' and E'' to the set value θ_{set} and E_{set}. Fig. 4(b) depicts the P_e-θ and I-θ curves in different state. Note that they are the function of the phase angle θ_{vsg} instead of the power angle δ. The green solid lines represent the initial state, and point a is the initial steady-state equilibrium point. VSG reaches a new equilibrium point a' from point a during fault state, when the new power balance is implemented by the application of P_0' and K_q'. And its output current also reaches a steady-state value as I_{set}. Similarly, the equilibrium point is moved from a' to a'' after fault clearance with the provided P_0'' and K_q'', while the internal voltage is controlled as E_{set}=E_0. Finally, it returns to the initial point a in normal state after line reclosing. As far as we can see, with the designed parameters applied in different states, θ_{vsg} keeps its original value throughout. And the movement of the operating points is only in a vertical line with the unchanged θ_{vsg}. Thus, the movement of operating points can always meet the requirements of current limitation in fault state and voltage recovery in O/S state, while the transient angle stability is achieved at the same time.

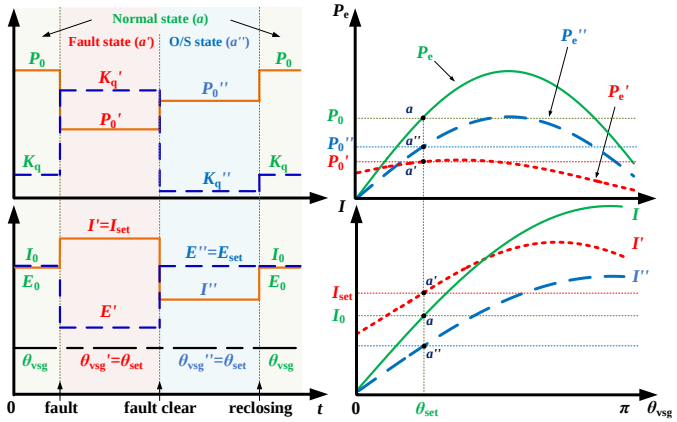

Fig. 4. The variation of system parameters during normal state, fault state and O/S state: (a) The change of P_0, K_q, I, E, θ_{vsg} during transient process and (b) The curves of P_e, I with θ_{vsg}.

Note that the instantaneous inrush current of VSG includes both the transient and steady-state components. Only the steady-state current limitation is considered in the proposed method since power converters can cope with overcurrent lasting for no longer than 20 ms, which usually does no harm to the converter valve [14]. Thus, the output current limit is set to I_{set}=1.2 pu during fault state and the internal voltage is set to E_{set}=1.0 pu after fault clearance in this paper.

However, it is an open loop control if only P_0 and K_q are modified. The control accuracy and stability of the VSG after the modification of P_0 and K_q are not reliable if there is any other disturbance. Besides, there are also errors brought from the fault location, and the difference between the distributed and lumped parameters. Thus, an additional feedback control is needed whose role is to fix the power imbalance and maintains the equilibrium. To achieve that, ΔP is added in the active power loop and regulated by detecting the feedback of the change tendency of $\Delta\delta$ and $d(\Delta\delta)/dt$. Note that the modification of P_0 and K_q have already provided a new post-fault operating point for the feedback control, where the phase angle θ_{vsg} is very close to the set value θ_{set}. Therefore, P_0 only needs to be regulated slightly with a small ΔP, which means the regulation would not make a big fluctuation. The feedback control can be mathematically expressed as:

$$J\ddot{\delta} = -D\dot{\delta} + (P_0 + \Delta P - P_e) \tag{23}$$

where

$$\Delta P = \begin{cases} +p, & (\Delta\delta < 0)\,\&\,(d\Delta\delta/dt < 0) \\ -p, & (\Delta\delta > 0)\,\&\,(d\Delta\delta/dt > 0) \end{cases} \tag{24}$$

According to (23)-(24), to track the change tendency of δ, $\Delta\delta$ and $d(\Delta\delta)/dt$ are detected and compared with zero. Note that a small positive threshold values for the better noise immunity is not necessary here, since the fluctuation of δ is usually smaller than power. The adjustment coefficient p of the additional feedback control does not need to regulate often. Normally, the required regulation range of the feedback control is slight due to the accuracy of the TWs method, and p is set to a small value for the accurate feedback regulation. Thus, p = 0.01 pu is adopted in this paper. Only under severe circumstances such as communication failure should p be set to a relatively large value to guarantee the transient stability.

C. Algorithm of the Proposed Method

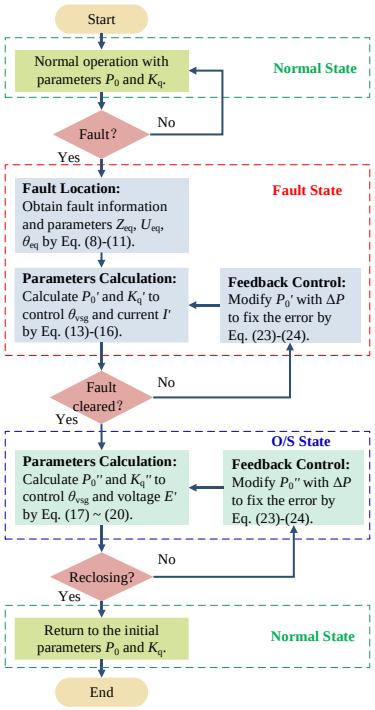

Fig. 5. Flow chart of the proposed method.

The flow chart of the proposed method is depicted in Fig. 5. In normal state, the initial parameters P_0, K_q are applied. When the fault is occurred, the fault information is obtained at first by (8)-(12). Then P_0', K_q' are calculated by (13)-(16) and adopted to control θ_{vsg} and I' to the set value in fault state,

while P_0' is further regulated by ΔP according to (24). Similarly, when the fault is cleared by tripping of line, P_0'', K_q'' are calculated by (17)-(20) and applied to control θ_{vsg} and E' to the set value in O/S state, while P_0'' is regulated by (24) as well. After line reclosing, P_0 and K_q should set to their initial values to make sure VSG can deliver the rated power in normal state.

In addition, the corresponding control logic is described as follows. When the VSG operates in normal state, $S_{1–3}$ in Fig.1 are at the position of logical 0. When fault is detected by the TWs-based detection unit, $S_{1–3}$ are switched from logic 0 to 1, and $S_{4–5}$ are switched to 0. When fault is cleared by tripping of line, $S_{4–5}$ are switched from 0 to 1. Finally, after line reclosing and VSG returns to normal state, $S_{1–3}$ are switched from 1 to 0. And the additional feedback control is removed after line reclosing by switching out S_3.

IV. Case Studies

In this Section, the validation of the proposed method is carried out by case studies. The robustness and feasible operating region for the proposed method are discussed as well. In addition, the application of the proposed method under asymmetric fault and for a multiple VSGs system are validated.

A. Validation of the Proposed Method

To analyze the effectiveness of the proposed method, two cases are carried out in the MATLAB/Simulink environment. The method in [20], which is an adaptive mode-switching control, is also analyzed as a comparison. The parameters of the VSG are given in Table I based on the guidelines in [14].

TABLE I
PARAMETERS OF THE INVESTIGATED SYSTEM

Parameters	Value	Parameters	Value
P_0	150 MW (1.0 pu)	ω_n	100π rad/s
Q_0	0	Z_T	0.01 pu
J	0.25 pu	L_f	0.2 pu
D	2 pu	C_f	0.15 pu
K_q	0.1 pu	r_1	0.2542 Ω/km
E_0	690 V	l_1	$2.287e^{-3}$ H/km
U_g	110 kV	c_1	$5.214e^{-9}$ F/km

Case 1: A three-phase-to-ground fault is occurred at t=0.5 s and cleared at t=1.5 s, while line reclosing at t=2.5 s. The line length is 60 km and fault point is at the 25% length of the line, while the fault impedance Z_f is 0.02 pu. According to Section II-C, the fault information is obtained by the TWs method. Arrive times of the initial and second TWs at the VSG end are t_{l1}=52 us and t_{l2}=156 us. Then the fault distances are calculated as m=14.78 km and n=45.22 km by (8). And the fault impedance is calculated as Z_f=0.026 pu by (10). Thereby, the modified control parameters are calculated as P_0'=0.3744 pu and K_q'=1.1877 pu during fault state by (15)-(16), to keep the original θ_{vsg} and the current limitation of 1.2 pu. Besides, P_0''=0.5753 pu and K_q''=0 pu after fault clearance by (19)-(20), to keep the original θ_{vsg} and the terminal voltage of 1.0 pu.

Fig. 6 shows the dynamics of VSG during the transient process in case 1 with different control strategies. As shown in Fig. 6(a), when the fault occurs without any control, the phase angle of VSG is divergent, which means the VSG loses the transient stability. And the post-fault output current of VSG is increased suddenly, which is well over the limitation. In Fig. 6(b), with a mode-adaptive control in [20], though the VSG does not totally lose the synchronization, the phase angle still oscillates in a bounded manner which leads to a large power oscillation. The system does not reach a true stable equilibrium point. Besides, the fault current of VSG cannot be limited in this method neither, which means this method is not acceptable in such a serve fault. As a comparison in Fig. 6(c), with the proposed method, the system can reach a stable equilibrium point fast and stable. In addition, the post-fault output current of VSG can reach the given current limit 1.2 pu fast during fault state. Only a short current spike lasting for no longer than 20 ms is observed on the VSG's current at the initial stage of the fault, which usually does no harm to the converter valve [14]. Compared with the method in [20] where only the active power loop is used for control, the proposed method uses two degrees of freedom of both the active and reactive power loops, to achieve both the transient stability enhancement and the steady-state current limitation at the same time during fault state, which brings better control performance.

In addition, the VSG is transient stable even without control after fault clearance at 1.5 s since the line length is short in case 1. Thus, the control in [20] is inactive during O/S state in case 1. However, the internal voltage of VSG is not recovered, which cannot provide the voltage support for power system. As shown in Fig. 6(c), due to the proposed method, the terminal voltage of VSG reaches the given value 1.0 pu during O/S state. Finally, the system returns to the normal state by line reclosing at 2.5 s and the control is then switched out.

$$P_0' = \begin{cases} P_0, & (S_{1\text{-}3}=0) \\ -\alpha' U_{eq}\left(U_{eq}\cos\delta_{set} + \sqrt{I_{set}^2(R'^2+X'^2) - U_{eq}^2\sin\delta_{set}^2}\right)\cos\delta_{set} + \beta' U_{eq}\left(U_{eq}\cos\delta_{set} + \sqrt{I_{set}^2(R'^2+X'^2) - U_{eq}^2\sin\delta_{set}^2}\right)\sin\delta_{set} & \\ +\alpha'\left[U_{eq}^2\cos\delta_{set}^2 + I_{set}^2(R'^2+X'^2) - U_{eq}^2\sin\delta_{set}^2 + 2U_{eq}\cos\delta_{set}\sqrt{I_{set}^2(R'^2+X'^2) - U_{eq}^2\sin\delta_{set}^2}\right], & (S_{1\text{-}3}=1)\,\&\,(S_{4\text{-}5}=0) \\ P_0'' = -\alpha'' U_g E_{set}\cos\delta'' + \beta'' U_g E_{set}\sin\delta_{set} + \alpha'' E_{set}^2, & (S_{1\text{-}3}=1)\,\&\,(S_{4\text{-}5}=1) \end{cases} \tag{21}$$

$$K_q' = \begin{cases} K_q, & (S_{1\text{-}3}=0) \\ \dfrac{U_n - \left(U_{eq}\cos\delta_{set} + \sqrt{I_{set}^2(R'^2+X'^2) - U_{eq}^2\sin\delta_{set}^2}\right)}{\beta'\left[U_{eq}^2\cos\delta_{set}^2 + I_{set}^2(R'^2+X'^2) - U_{eq}^2\sin\delta_{set}^2 + 2U_{eq}\cos\delta_{set}\sqrt{I_{set}^2(R'^2+X'^2) - U_{eq}^2\sin\delta_{set}^2}\right]}, & (S_{1\text{-}3}=1)\,\&\,(S_{4\text{-}5}=0) \\ \quad -U_{eq}(\alpha'\sin\delta_{set} + \beta'\cos\delta_{set})\left(U_{eq}\cos\delta_{set} + \sqrt{I_{set}^2(R'^2+X'^2) - U_{eq}^2\sin\delta_{set}^2}\right) - Q_0 & \\ K_q'' = \dfrac{U_n - E_{set}}{\beta'' E_{set}^2 - E_{set}U_g(\alpha''\sin\delta_{set} + \beta''\cos\delta_{set}) - Q_0}, & (S_{1\text{-}3}=1)\,\&\,(S_{4\text{-}5}=1) \end{cases} \tag{22}$$

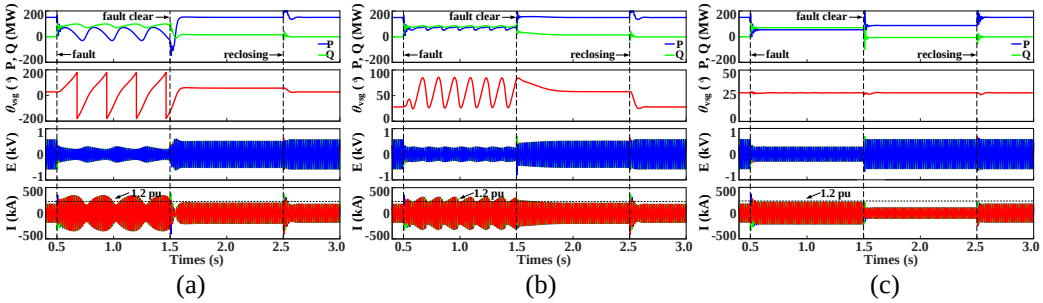

Fig. 6. Dynamics of VSG during the transient process in case 1: (a) without any control. (b) with the method in [20]. (c) with the proposed method.

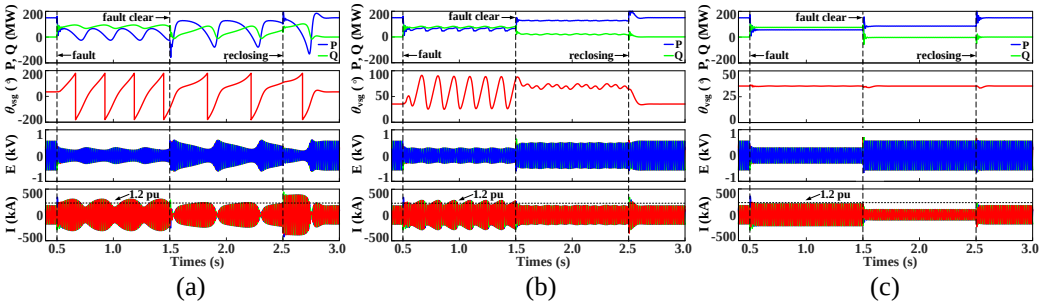

Fig. 7. Dynamics of VSG during the transient process in case 2: (a) without any control. (b) with the method in [20]. (c) with the proposed method.

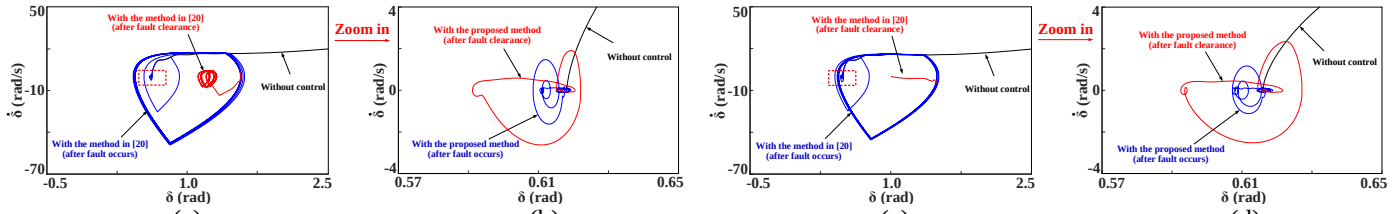

Fig. 8. Phase portrait of VSG during fault state and O/S state: (a) case 1: comparison with the method in [20] and without control. (b) case 1: comparison with the proposed method and without control. (c) case 2: comparison with the method in [20] and without control. (d) case 2: comparison with the proposed method and without control.

Case 2: A three-phase-to-ground fault is occurred at t=0.5 s and cleared at t=1.5 s, with line reclosing at t=2.5 s. Compared with case 1, the line length is increased to 80 km. Arrival times of the initial and second TWs at the VSG end are t_{l1}=69 us and t_{l2}=207 us. Then the fault distances are calculated as m=19.61 km and n=60.39 km. And the fault impedance is calculated as Z_f=0.025 pu. Thereby, the modified control parameters are calculated as P_0'=0.3926 pu and K_q'=0.9731 pu during fault state, to keep the original θ_{vsg} and the current limitation of 1.2 pu. And P_0''=0.5693 pu and K_q''=-0.0413 pu after fault clearance, to keep the original θ_{vsg} and the terminal voltage of 1.02 pu.

Fig. 7 shows the dynamics of VSG during the transient process in case 2 with different control strategies. Compared with case 1, the VSG still loses the transient stability without control even if the fault is cleared due to the rest of the line is longer than it in case 1. Compared with Fig. 7(a)-(c), the system can only reach a true stable equilibrium point during O/S state with the proposed method, which guarantees the system transient stability and the internal voltage at the meanwhile. Similarly, the transient stability and the fault current are controlled at the same time during fault state.

In addition, the VSG may face another problem. As shown in Fig. 7 (a)(b), the output current of VSG after the line reclosing is increased rapidly and exceeds the current limitation a lot. That is because there is a great phase angle difference of VSG compared with its original value, and then lead to a serve fluctuation. This overcurrent cannot be solved by method [20] since it also produces an oscillation of phase angle. For a comparison, the proposed method is acceptable to handle this problem. Since the phase angle of VSG maintains its original value during the whole transient process, and thus the transient fluctuation after line reclosing decays fast.

TABLE II
COMPARISON OF THE METHODS

Methods	Change PQ reference [7][8]	Change inertia, damping [9][10]	Mode-switching [20]	Proposed method
Improve stability during fault state	Yes	Yes	Yes	Yes
Current limit during fault state	No	No	No	Yes
Improve stability after fault clear	No	No	Yes	Yes
Voltage support after fault clear	No	No	No	Yes
Achieve precise control effect	No	No	No	Yes

Moreover, phase portrait curves in Fig. 8(a)-(d) support the simulation results. The transient stability can be analyzed intuitively by the phase portrait curve, which describes the relationship between power angle and the angular speed. With the method in [20], though the power angle is not divergent,

the moving range of the phase portrait is large since the angle is oscillated. To be compared, when the proposed method is adopted, the power angle is almost convergent and stable.

The comparison between the proposed method and existing methods is shown in Table II. All the methods can improve the transient stability of VSG. However, only the proposed method can achieve the accurately and simultaneously control of the transient stability while considering the current limiting during fault state and the voltage support after fault clearance.

B. Robustness to Parameter Mismatch

Note that there is normally parameter mismatch, which may origin from the error in the fault information measurement, communication failure, parameters calculation, use of the lumped parameters, and control delays in practice. Therefore, the robustness to parameters mismatch should be considered.

In case 2, P_0'=0.3926 pu and K_q'=0.9731 pu during fault state. Though P_0' and K_q' provide a new post-fault steady-state operating point during fault state, it will be easy interfered by the disturbances origin form the above errors. To be compared, with the completely precise condition, the parameters should be P_0'=0.3776 pu and K_q'=0.9412 pu, which have errors about 4%. P_0'' and K_q'' have no calculation error due to the fault information is not needed in O/S state. Besides the error from the fault information acquisition, the use of the lumped parameters of line also brings the error compared with the distributed parameters. Thus, the simplification of the line parameters should be verified as well.

Although there are parameter mismatch, the control performance can still be achieved due to the influence of the feedback control introduced in (23)-(24). As shown in Fig. 8(b) and (d), with the use of the feedback control, the phase portraits curves of VSG finally run into a very small circle with the influence of ΔP, which is very close to the precisely stable equilibrium point. To validate the anti-error ability of the proposed method, the line is then modelled as the distributed parameters with the parameter mismatch origins from the above errors. Under that condition, the dynamics of VSG in case 2 with the proposed method is shown in Fig. 9. Compared with Fig. 7(c), the fluctuation of variables is large with the consideration of parameter mismatch, especially the internal voltage during fault state. The error mainly origins from the influence of the distributed capacitance. However, the proposed method is still effective due to the feedback control.

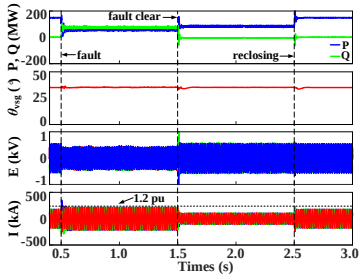

Fig. 9. Dynamics of VSG during the transient process in case 2 with the distributed parameters of line and the parameter mismatch.

In addition, the delays of fault location and VSG control are inevitable in practice. The total delays are usually around hundreds of microseconds. Yet, it is much less than the response time of power loops, which is usually longer than 100 ms [9]. Since the transient stability of the VSG is determined by power loops, the influence of these delays can be negligible.

In short, errors origin from fault information measurement, communication failure, parameters calculation, use of the lumped parameters, and the control delays in this paper. However, the proposed method still applies considering these errors due to the effect of the additional feedback control.

C. Feasible Operating Region Analysis of the Method

The proposed method is validated by simulation results. In the most of fault conditions, this method can achieve its control objectives. However, when the worst faults such as a solid fault occurs near the terminal of VSG, both the active and reactive power loops may exceed their control margin, and then the method may be ineffective. Thus, it's necessary to analyze the feasible region of the method during fault state.

The output current of VSG during fault state is derived as (13), which is related to the VSG's internal voltage E, equivalent impedance R', X' and equivalent voltage $\boldsymbol{U}_{\mathbf{eq}}$. To achieve the better control performance, the fault current should be restricted to I_{set}, while the phase angle θ_{vsg} keeps its initial value, which means only the VSG's internal voltage E can be used for regulation under a specific fault condition. However, when the fault point is very close to VSG's terminal and the fault impedance is small, the system equivalent impedance R', X' are small due to (12), which may lead to the exceeding of fault current even though E is regulated to a very small value. Obviously, it is not reasonable for the steady operation of VSG. Therefore, the feasible region of the method is expressed as the reasonable variation range of E, with the related fault impedance Z_f and fault location k (k=0 and 1 represent the fault at VSG's and grid's terminals respectively) in different fault condition.

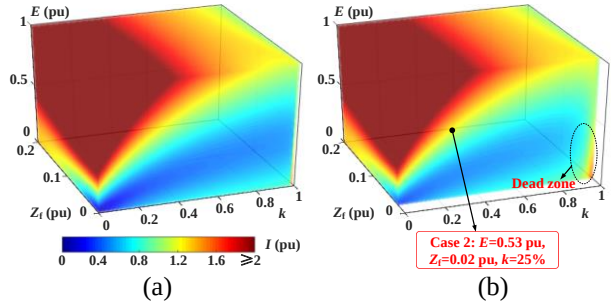

Fig. 10. Feasible region of the method during fault state with: (a) a 4-D graph of current with the change of E, Z_f and k and (b) the cross section at Z_f=0.02 pu.

Thus, a 4-D graph depicted in Fig. 10 is used to analyze the feasible region of the method. The colour represents the magnitude of fault current, which is decided jointly by E, k and Z_f. It can be observed that the fault current has a negative correlation with the value of k and Z_f, while it has a positive correlation with the value of E. Among them, k and Z_f represent the fault information, which cannot be controlled. In terms of a specific fault condition with the fixed k and Z_f, only E can be regulated to control the related fault current through the proposed method. And if there exists an appropriate value of E which makes the related fault current below the limit value, then the proposed method is feasible under that fault condition. Otherwise, the proposed method is ineffective under

that fault condition. Note that there is a dead zone with an abnormal change tendency in the lower right corner in Fig. 10(b), which is caused by the infinite value in the denominator in (13) when k is near 1. However, this zone is not necessary to consider since E cannot be very low in practice when the fault point is very close to the grid.

As shown in Fig. 10(a), even if a solid fault occurs near the VSG's terminal, there is still a region where the fault current below the limit value 1.2 pu with the regulation of E, which means the feasible region of the proposed method is large enough for the severe fault. However, under such extreme condition, the control performance is achieved at the cost of the drop of the VSG's internal voltage during fault state, which is not always suitable and requires a trade-off.

Overall, the feasible region of the method is large enough during fault state for the application in most of fault conditions. And the proposed method can be used in any types of symmetrical faults, such as the grid voltage dips, three-phase-to-ground fault and tripping of line. Nevertheless, the application of the proposed method under unbalanced condition and in a multiple VSGs system is concerned as well, which is further studied in next subsections.

D. Validation of the Proposed Method under Asymmetrical Fault

The symmetrical three-phase-to-ground fault are mainly analyzed as they are more severe than other asymmetrical faults. However, the asymmetrical faults are more common, which should be concerned as well. When VSG operates under unbalanced condition caused by an asymmetric fault, the unbalanced voltage and current can be decomposed into the sum of the positive, negative and zero sequence component due to the symmetrical component method. Since the topology used in this paper is a three-phase three-wire system, the zero-sequence component is not considered. Note that the proposed method still applies, while the only difference is that the symmetrical components theory should first be used and the positive component is extracted for the control of the proposed method.

Under unbalanced condition, the output power of VSG can be decomposed into the average component and the double frequency-oscillating component. The expression of the average power can be expressed as

$$\begin{cases} P_e^+ = u_d^+ i_d^+ + u_q^+ i_q^+ \\ Q_e^+ = -u_d^+ i_q^+ + u_q^+ i_d^+ \end{cases} \tag{25}$$

where u_{dq}, i_{dq} are the measured output voltage and current of VSG in dq frame. The superscript +, - represent the positive and negative sequence components respectively.

If the negative sequence component is not controlled in the VSG algorithm under asymmetrical fault, the fluctuation is existed in output voltage, current and power due to the influence of u_{dq}^- and i_{dq}^-, which is not conducive to system operation. In order to improve the performance under unbalanced condition, there are three primary objectives of VSG, which are the balanced current control, and the suppression of active power or reactive power. However, the above objectives cannot be realized at the same time since the different treatment of the negative sequence current. Normally, the current quality and current limitation of VSG is of primarily concerned.

The power calculation of VSG under unbalanced condition is shown in Fig. 11(a), where the positive u_{dq}^+ and i_{dq}^+ are exacted and then the positive power is obtained. The sequence separation can be realized by second-order generalized integrator (SOGI), which is designed in detail in [28], [29]. The inner voltage and current loops control under unbalanced condition is shown in Fig. 11(b), where the inner loops can be divided into two parts: the positive and negative sequence inner loops control. The positive sequence voltage and current loops are used to track the voltage reference while negative sequence current loop is used to eliminate the negative sequence current by setting the negative current reference to zero.

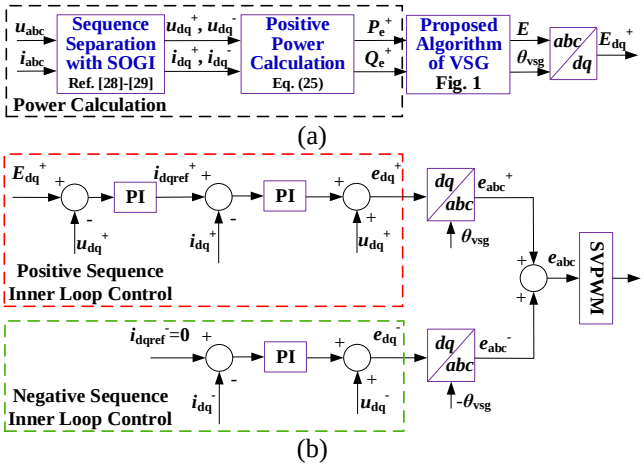

Fig. 11. VSG control strategy under asymmetric fault: (a) Sampling (b) positive and negative inner loop control.

The balanced current control is needed as an important prerequisite of the proposed method under asymmetrical fault. With the balanced current control, the application of the proposed method under both symmetrical and asymmetrical faults are the same, since only the positive sequence components exist in the VSG algorithm. Therefore, there is no need to change the algorithm of the proposed method in Fig. 5. Correspondingly, the equivalent system circuit under asymmetrical fault is still derived as (11) with the positive fault voltage $\boldsymbol{U}_f^+$ at the fault point. In particular, as to a single line-to-ground fault, $\boldsymbol{U}_f^+$ can be further derived by the sequence networks method.

$$\begin{cases} \boldsymbol{U}_f^+ = \boldsymbol{U}_{f0} - \dfrac{\boldsymbol{U}_{f0} Z_F}{3Z_F - 3Z_f} \\ Z_F = \dfrac{(Z_1 + Z_{21}) Z_{22}}{2Z_1} \end{cases} \tag{26}$$

where, $\boldsymbol{U}_{f0}$ is the initial voltage at the fault point, Z_F is the input impedance from the fault point. Then the following steps to design P_0' and K_q' during fault state are the same as symmetrical fault based on (13)-(16). Besides, the design process after tripping of line during O/S state is the same as (17)-(20).

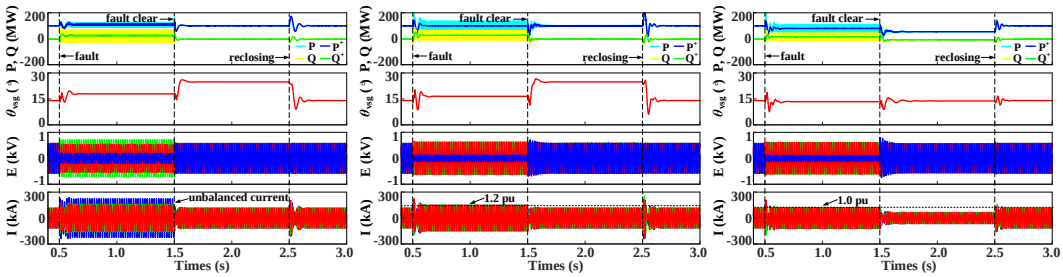

Fig. 12. Dynamics of VSG during the transient process in case 3: (a) without any control. (b) with the balanced current control in [29]. (c) with the proposed method.

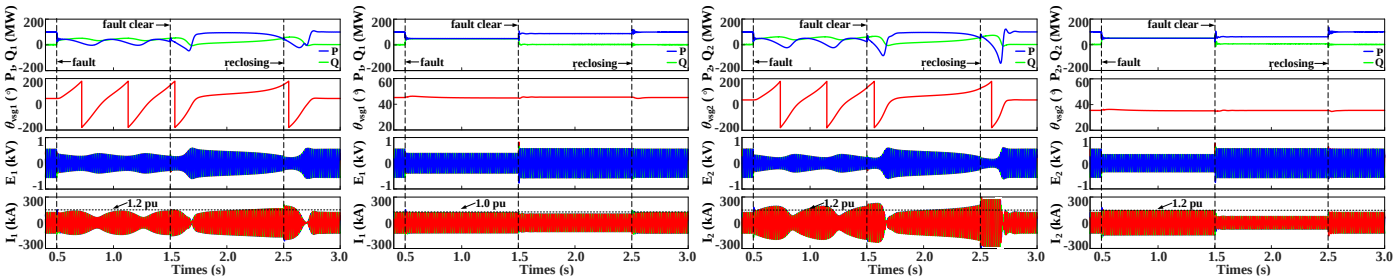

Fig. 14. Dynamics of VSGs during the transient process in case 4: (a) VSG1 without any control. (b) VSG1 with the proposed method. (c) VSG2 without any control. (d) VSG2 with the proposed method.

It is important to note that the control strategy under unbalanced condition is also suitable for the symmetrical condition, which means the control scheme in Fig. 11 does not need to change during normal state and symmetrical fault state. The negative components are zero under balanced condition and thus the negative inner loops control is inactive automatically. To better validate the effectiveness of the proposed method under asymmetrical fault, the following case is studied with the comparison of the balanced current control and the proposed method.

Case 3: A single-line-to-ground fault is occurred at t=0.5 s and cleared at t=1.5 s, while line reclosing at t=2.5 s. The output active power is set to 100 MW. The line length is 60 km and fault point is at the 1/6 length of the line, while the fault impedance Z_f is 0.02 pu. The fault information acquisition is similar with case 1. With the positive sequence components extraction, the modified control parameters are calculated as P_0'=0.7756 pu and K_q'=0.6643 pu during fault state, to keep the original θ_{vsg} and the current limitation of 1.0 pu. And P_0''=0.5213 pu and K_q''=0 pu after fault clearance, to keep the original θ_{vsg} and the terminal voltage of 1.0 pu.

Fig. 12 shows the dynamics of VSG under a single line-to-ground fault with different control strategies. As shown in Fig. 12(a), when the fault occurs without any control, the phase angle of VSG is increased. But the transient stability of VSG is not lost even the fault point is very close to the VSG terminal. Besides, the output voltage and current of VSG are distorted due to the unbalanced condition. In Fig. 12(b), with the balanced current control in [29], the current of VSG is balanced and does not exceed the limitation of 1.2 pu. That is because the severity of the single-line-to-ground fault is smaller than the symmetrical three-phase-to-ground fault. However, the voltage is still distorted which leads to a power oscillation. Note that the suppression of power fluctuation and balanced current are a pair of contradiction. As a comparison in Fig. 12(c), the better transient performance is achieved with the proposed method. The post-fault output current of VSG can further reach the smaller current limitation of 1.0 pu during fault state, that is, the rated current. Besides, the control performance during O/S state is the same as the case of symmetrical fault since the fault is cleared.

E. Validation of the Proposed Method for a Multiple VSGs System

When a system with multiple generators is considered instead of the single-machine infinite-bus system, the generators are integrated to PCC whose voltage and phase angle are fluctuated compared with the idea grid. As for the generators, PCC operates at a new equilibrium point after fault. To further validate the applicability and effectiveness of the proposed method in a system with multiple generators, a grid-connected system that consists of two VSGs is studied. The system topology is shown in Fig. 13, and the relevant detailed parameters are given in Table III. Note that the lines in the system are still the parallel-circuit lines. The line length is set as 60 km and 80 km in case 1 and 2, respectively. To better analyse the influence of the line length, the length range of lines in a multiple VSGs system is set from 40 km to 160 km.

As for each VSG in the multiple VSGs system, the control algorithm of the proposed method is the same. The only difference lies in the derivation of the equivalent voltage $\boldsymbol{U}_{eq}$ and impedance Z_{eq} for the parameters calculation of each VSG. The topology in Fig. 13 can be further simplified as the green block through the delta-star transformation and the Thévenin theorem, where the equivalent impedance of VSGs can be derived as

$$\begin{cases} Z_{\mathrm{eq1}} = \dfrac{Z_{\mathrm{a}} Z_{\mathrm{b}}}{Z_{\mathrm{a}} + Z_{\mathrm{b}} + Z_{\mathrm{c}}} + Z_{\mathrm{T1}} \\ Z_{\mathrm{eq2}} = \dfrac{Z_{\mathrm{a}} Z_{\mathrm{c}}}{Z_{\mathrm{a}} + Z_{\mathrm{b}} + Z_{\mathrm{c}}} + Z_{\mathrm{T2}} \end{cases} \tag{27}$$

where Z_{a}, Z_{b}, Z_{c} and Z_{d} represent the line impedance in the system. Z_{T1}, Z_{T2} represent the transformer's leakage impedance of VSGs. Besides, the equivalent voltage $\boldsymbol{U}_{\mathbf{eq}}$ can be obtained based on circuit principle with the set value of current limitation of VSGs. Thereby, the control of VSG1 and VSG2 are both complied with the algorithm of the proposed method in Fig. 5.

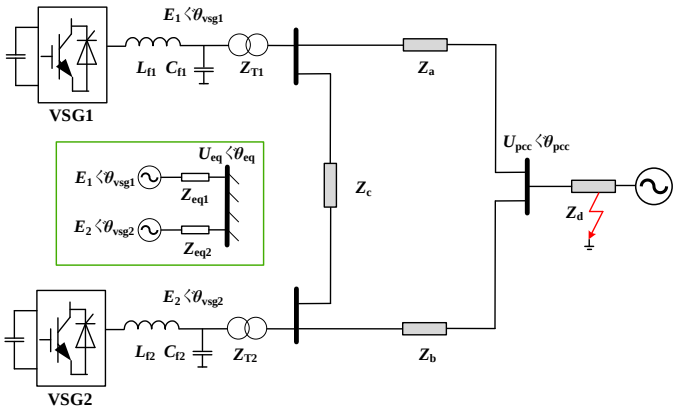

Fig. 13. Topology of parallel operation of two VSGs connected to a grid.

Note that a system with multiple VSGs is studied in this subsection. In particular, as for a large-scale power system, the PCC voltage would not be affected too much during fault state compared to it in a small-scale system, while the PCC voltage can be supported by distributed energy resources [30], [31]. Therefore, the PCC voltage can be directly used as the equivalent voltage for the parameters design in a large-scale power system.

TABLE III
PARAMETERS OF THE MULTIPLE GENERATORS SYSTEM

Parameters	Value	Parameters	Value
P_1/P_2	100 MW	$Z_{\mathrm{T1}}/Z_{\mathrm{T1}}$	0.10/0.04 pu
Q_1/Q_2	0/0 MW	$L_{\mathrm{f1}}/L_{\mathrm{f2}}$	0.2 pu
J_1/J_2	0.3/0.2 pu	$C_{\mathrm{f1}}/C_{\mathrm{f2}}$	0.15 pu
D_1/D_2	2/1 pu	*Length of* Z_{a}	160 km
$K_{\mathrm{q1}}/K_{\mathrm{q2}}$	0.2/0.1 pu	*Length of* Z_{b}	80 km
E_1/E_2	690 V	*Length of* Z_{c}	160 km
U_{g}	110 kV	*Length of* Z_{d}	40 km

Case 4: A three-phase-to-ground fault is occurred at t=0.5 s and cleared at t=1.5 s, while line reclosing at t=2.5 s. The fault point is at the 1/4 length of the line of Z_{d}, while the fault impedance Z_{f} is 0.02 pu. Note that the distance between VSG1 and the fault point is large, therefore, the current limitation can be set to the rated value 1.0 pu during fault state, while the terminal voltage can be set to 1.02 pu during O/S state which is slightly higher than the rated value. The distance between VSG2 and the fault point is relatively short, and thus the current limitation and voltage are set to 1.2 pu and 1.0 pu respectively during two states. The modified control parameters of VSG1 are calculated as P_0'= 0.4920 pu and K_{q}'= 0.6726 pu during fault state, and P_0''=0.8799 pu and K_{q}''=-0.3367 pu after fault clearance. As for VSG2, P_0'= 0.5091 pu and K_{q}'= 0.7980 pu during fault state, and P_0''=0.6209 pu and K_{q}''=0 pu after fault clearance.

Fig. 14 shows the dynamics of two VSGs during the transient process. As shown in Fig. 14(a) and (c), when the fault occurs without any control, the transient stability of both VSG1 and VSG2 is lost. Besides, the current of VSG2 exceeds the limitation of 1.2 pu. In Fig. 14(b) and (d), with the proposed method, the current of both VSG1 and VSG2 during fault state can be limited to the set values of 1.0 pu and 1.2 pu respectively. Besides, the terminal voltage of both VSG1 and VSG2 during O/S state are controlled to the set values of 1.02 pu and 1.0 pu respectively. That is, the proposed method is also applicable for a multiple VSGs system.

V. CONCLUSIONS

This paper explores how to improve the transient angle stability of VSG while considering the current limitation during fault state and voltage support after fault clearance. At first, the post-fault large-signal models of VSG are established with the fault information acquired by TWs method. Then a two-stage simultaneous control scheme is proposed, which is fulfilled by mode switching and an additional feedback control based on the fault signal. With the proposed method, the phase angle of VSG can remain its set value while the steady-state current can be limited to the required value during fault state. Similarly, the phase angle and internal voltage of VSG can also be controlled at the meanwhile during O/S state. The VSG can achieve the better performance during transient process with the proposed method, which is validated by the simulation results. In addition, the practicality and effectiveness of this method are also discussed by the analysis of robustness to parameter mismatch and the analysis of the feasible operating region. Last but not least, the application of the proposed method for asymmetric fault and for multiple VSGs is validated as well.

REFERENCES

[1] Q. Zhong and G. Weiss, "Synchronverters: Inverters that mimic synchronous generators," *IEEE Trans. Ind. Electron.*, vol. 58, no. 4, pp. 1259-1267, Apr. 2011.

[2] Q. Zhong, P. Nguyen, Z. Ma, and W. Sheng, "Self-synchronized synchronverters: inverters without a dedicated synchronization unit," *IEEE Trans. Power Electron.*, vol. 29, no. 2, pp. 617-630, Feb. 2014.

[3] Z. Shuai, W. Huang, C. Shen, J. Ge, and J. Shen, "Characteristics and restraining method of fast transient inrush fault currents in synchronverters," *IEEE Trans. Ind. Electron.*, vol. 64, no. 9, pp. 7487-7497, Sep. 2017.

[4] H. Xin, L. Huang, L. Zhang, Z. Wang, and J. Hu, "Synchronous instability mechanism of P-f droop-controlled voltage source converter caused by current saturation," *IEEE Trans. Power Syst.*, vol. 31, pp. 5206-5207, Feb. 2016.

[5] H. Wu, X. Ruan, D. Yang, X. Chen, W. Zhao, Z. Lv, and Q.-C. Zhong, "Small-signal modeling and parameters design for virtual synchronous generators," *IEEE Trans. Ind. Electron.*, vol. 63, no. 7, pp. 4292-4303, Jul. 2016.

[6] X. Wang, M. G. Taul, H. Wu, Y. Liao, F. Blaabjerg, and L. Harnefors, "Grid-synchronization stability of converter-based resources an overview," *IEEE Open J. Ind. Appl.*, vol. 1, pp. 115-134, Aug. 2020.

[7] Z. Shuai, C. Shen, X. Liu, Z. Li, and Z. Shen, "Transient angle stability of virtual synchronous generators using Lyapunov's direct method," *IEEE Trans. Smart Grid*, vol. 10, no. 4, pp. 4648-4661, Jul. 2019.

[8] D. Pan, X. Wang, F. Liu, and R. Shi, "Transient stability impact of reactive power control on grid-connected converters," in *Proc. IEEE Energy Convers. Congr. Expo.*, pp. 4311-4316, Oct. 2019.

[9] D. Pan, X. Wang, F. Liu, and R. Shi, "Transient stability of voltage-source converters with grid-forming control: a design - oriented study,"

IEEE J. Emerg. Sel. Topics Power Electron., vol. 8, no. 2, pp. 1019-1033, Jun. 2020.

[10] J. Alipoor, Y. Miura, and T. Ise, "Power system stabilization using virtual synchronous generator with alternating moment of inertia," *IEEE J. Emerg. Sel. Top. Power Electron.*, vol. 3, no. 2, pp. 451-458, Jun. 2015.

[11] H. Cheng, Z. Shuai, C. Shen, X. Liu, Z. Li, and Z. Shen, "Transient angle stability of paralleled synchronous and virtual synchronous generators in islanded microgrids," *IEEE Trans. Power Electron.*, vol. 35, no. 8, pp. 8751-8765, Aug. 2020.

[12] J. Alipoor, Y. Miura, and T. Ise, "Stability assessment and optimization methods for microgrid with multiple VSG units," *IEEE Trans. Smart Grid*, vol. 9, no. 2, pp. 1462-1471, Mar. 2018.

[13] Chen, F. Prystupczuk, and T. O'Donnell, "Use of voltage limits for current limitations in grid-forming converters," *CSEE J. Power Energy Syst.*, vol. 6, no. 2, pp. 259-269, Jun. 2020.

[14] L. Zhang, L. Harnefors, and H. P. Nee, "Power-synchronization control of grid-connected voltage-source converters," *IEEE Trans. Power Syst.*, vol. 25, no. 2, pp. 809-820, May 2010.

[15] L. Huang, H. Xin, Z. Wang, L. Zhang, K. Wu, and J. Hu, "Transient stability analysis and control design of droop-controlled voltage source converters considering current limitation," *IEEE Trans. Smart Grid*, vol. 10, no. 1, pp. 578-591, Jan. 2019.

[16] A. D. Paquette and D. M. Divan, "Virtual impedance current limiting for inverters in microgrids with synchronous generators," *IEEE Trans. Ind. Appl.*, vol. 51, no. 2, pp. 1630-1638, Mar. 2015.

[17] A. Gkountaras, S. Dieckerhoff, and T. Sezi, "Evaluation of current limiting methods for grid forming inverters in medium voltage microgrids," in *Proc. IEEE Energy Convers. Congr. Expo.*, pp. 1223-1230, Sep. 2015.

[18] M. G. Taul, X. Wang, P. Davari, and F. Blaabjerg, "Current limiting control with enhanced dynamics of grid-forming converters during fault conditions," *IEEE J. Emerg. Sel. Top. Power Electron.*, vol. 8, no. 2, pp. 1062-1073, Jun. 2019.

[19] T. Qoria, F. Gruson, F. Colas, G. Denis, T. Prevost, and X. Guillaud, "Critical clearing time determination and enhancement of grid-forming converters embedding virtual impedance as current limitation algorithm," *IEEE J. Emerg. Sel. Top. Power Electron.*, vol. 8, no. 2, pp. 1050-1061, Jun. 2020.

[20] H. Wu and X. Wang, "A mode-adaptive power-angle control method for transient stability enhancement of virtual synchronous generators," *IEEE J. Emerg. Sel. Top. Power Electron.*, vol. 8, no. 2, pp. 1034-1049, Jun. 2020.

[21] H. Yuan, X. Yuan, and J. Hu, "Modeling of grid-connected VSCs for power system small-signal stability analysis in DC-link voltage control timescale," *IEEE Trans. Power Syst.*, vol. 32, no. 5, pp. 3981-3991, Sep. 2017.

[22] L. Harnefors, X. Wang, A. Yepes, and F. Blaabjerg, "Passivity-based stability assessment of grid-connected VSCs -an overview," *IEEE J. Emerg. Sel. Top. Power Electron.*, vol. 4, no. 1, pp. 116-125, Mar. 2016.

[23] O. D. Naidu and A. K. Pradhan, "Precise traveling wave based transmission line fault location method using single-ended data," *IEEE Trans. Ind. Inform.*, vol. 17, no. 8, pp. 5197-5207, Aug. 2021.

[24] S. Yang, W. Xiang, M. Zhou, W. Zuo, and J. Wen, "A single-end protection scheme for hybrid MMC-HVDC grids considering the impacts of the active fault current-limiting control", *IEEE Trans. Power Del.*, vol. 36, no. 4, pp. 2001-2013, Aug. 2021.

[25] H. A. A. el-Ghany, A. M. Azmy, and A. M. Abeid, "A general travelling-wave based scheme for locating simultaneous faults in transmission lines", *IEEE Trans. Power Del.*, vol. 35, no. 1, pp. 130-139, Feb. 2020.

[26] X. He, H. Geng, J. Xi, and J. M. Guerrero, ''Resynchronization analysis and improvement of grid-connected VSCs during grid faults,'' *IEEE J. Emerg. Sel. Top. Power Electron.*, vol. 9, no. 1, pp. 438-450, Feb. 2021.

[27] R. Sgarbossa, S. Lissandron, P. Mattavelli, R. Turri, and A. Cerretti, "Analysis of ΔP-ΔQ area of uncontrolled islanding in low-voltage grids with PV generators," *IEEE Trans. Ind. Appl.*, vol. 52, no.3, pp. 2387-2396, May. 2016.

[28] P. Rodr ́guez, A. Luna, I. Candela, R. Mujal, R. Teodorescu, and F. Blaabjerg, "Multi-resonant frequency-locked loop for grid synchronization of power converters under distorted grid conditions," *IEEE Trans. Ind. Electron.*, vol. 58, no. 1, pp. 127-138, Jan. 2011.

[29] M. Chen, X. Xiao, C. Yuan, and S. Tao, "Flexible power control of virtual synchronous generators under unbalanced grid voltage conditions," in *Proc. IEEE Energy Convers. Congr. Expo.*, pp. 2881-2888, Oct. 2017.

[30] V. Saxena, N. Kumar, B. Singh, and B. Panigrahi, "A voltage support control strategy for grid integrated solar PV system during abnormal grid conditions utilizing interweaved GI," *IEEE Trans. Ind. Electron.*, vol. 68, no. 9, pp. 8149-8157, Sep. 2021.

[31] T. Fons ̃ca, R. L. A. Ribeiro, T. O. A. Rocha, F. B. Costa, and J. M. Guerrero, "Voltage grid supporting by using variable structure adaptive virtual impedance for LCL-voltage source converter DG converters," *IEEE Trans. Ind. Electron.*, vol. 67, no. 11, pp. 9326-9336, Nov. 2020.

Kun Sun received the B.S. and M.Sc. degrees in electrical engineering from Huazhong University of Science and Technology (HUST), Wuhan, China, in 2015 and 2018, respectively. From 2019 to 2020, he was a Visiting Ph.D. Student with the Department of Energy Technology, Aalborg University, Aalborg, Denmark. He is currently working toward the Ph.D. degree in electrical engineering at HUST. His current research interests include stability analysis and control of renewable energy integration.

Wei Yao (Senior Member, IEEE) received the B.S. and Ph.D. degrees in electrical engineering from Huazhong University of Science and Technology (HUST), Wuhan, China, in 2004 and 2010, respectively. He was a Post-Doctoral Researcher with the Department of Power Engineering, HUST, from 2010 to 2012 and a Postdoctoral Research Associate with the Department of Electrical Engineering and Electronics, University of Liverpool, Liverpool, U.K., from 2012 to 2014. Currently, he has been a Professor with the School of Electrical and Electronics Engineering, HUST, Wuhan, China. His current research interests include stability analysis and control of smart grid, renewable energy integration, HVDC and DC Grid, and application of artificial intelligence in Smart Grid.

Jinyu Wen (Member, IEEE) received the B.S. and Ph.D. degrees in electrical engineering from Huazhong University of Science and Technology (HUST), Wuhan, China, in 1992 and 1998, respectively. He was a visiting student from 1996 to 1997 and a Research Fellow from 2002 to 2003 with the University of Liverpool, U.K., and a Senior Visiting Researcher with the University of Texas at Arlington, USA, in 2010. From 1998 to 2002, he was a Director Engineer with XJ Electric Company Ltd., China. In 2003, he joined HUST, where he is currently a Professor. His current research interests include renewable energy integration, energy storage application, DC grid, and power system operation and control.

Lin Jiang (Member, IEEE) received the B.Sc. and M.Sc. degrees from the Huazhong University of Science and Technology, Wuhan, China, in 1992 and 1996, respectively, and the Ph.D. degree from the University of Liverpool, Liverpool, U.K., in 2001, all in electrical engineering. He was a Postdoctoral Research Assistant with The University of Liverpool, Liverpool, U.K., from 2001 to 2003 and a Postdoctoral Research Associate with the Department of Automatic Control and Systems Engineering, University of Sheffield, Sheffield, U.K., from 2003 to 2005. He was a Senior Lecturer with the University of Glamorgan from 2005 to 2007 and joined the University of Liverpool in 2007. He is currently a Reader with the Department of Electrical Engineering and Electronics, The University of Liverpool. His current research interests include control and analysis of power system, smart grid, and renewable energy.